iScience

CellPress

Article

Sodium Dodecyl Sulfate Preferentially Promotes Enclathration of Methane in Mixed Methane-Tetrahydrofuran Hydrates

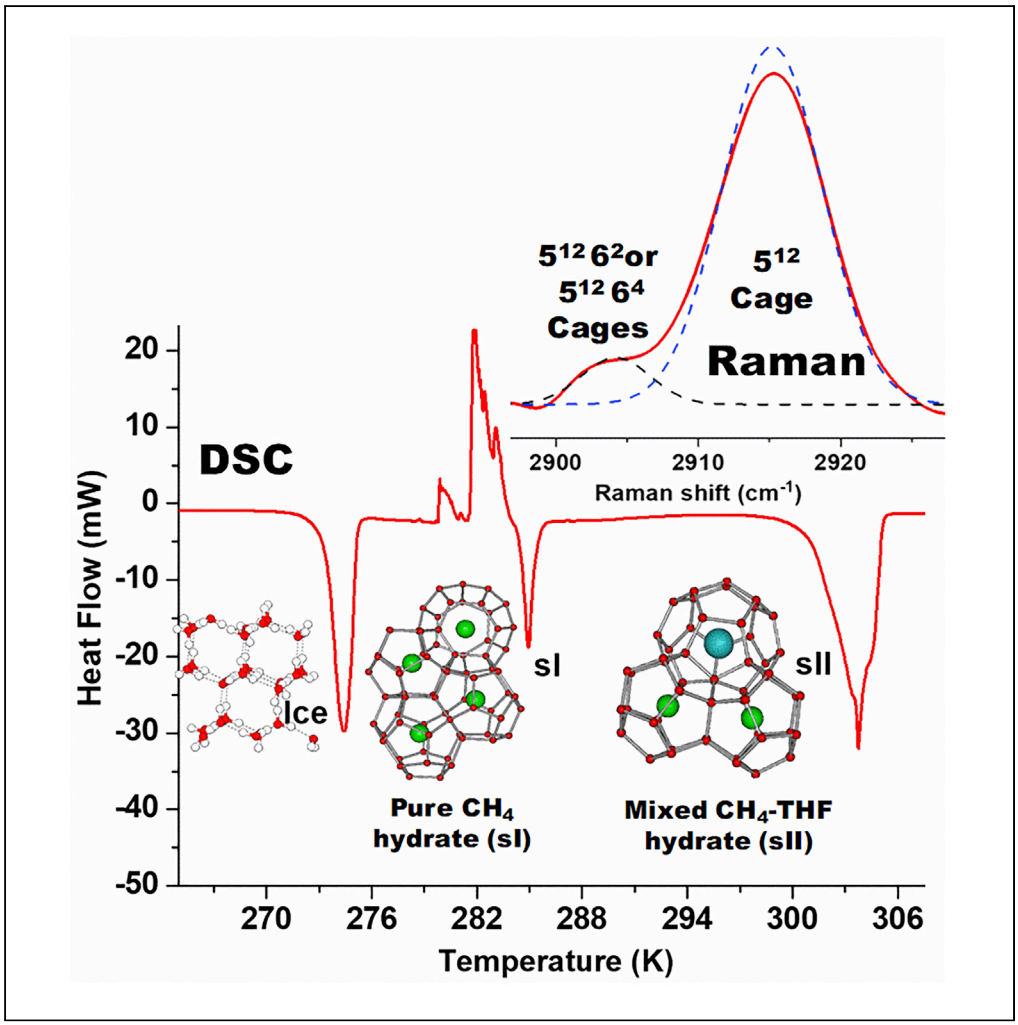

Asheesh Kumar, Rajnish Kumar, Praveen Linga

praveen.linga@nus.edu.sg

HIGHLIGHTS

Sodium dodecyl sulfate preferentially promotes structure I hydrates

Co-existence of pure CH_4 (sI) and mixed CH_4-THF hydrates (sII) in the presence of SDS

Temperature-dependent CH_4 occupancy in small and large cages of mixed hydrates

Kumar et al., iScience *14*, 136–146
April 26, 2019
https://doi.org/10.1016/j.isci.2019.03.020

iScience

CellPress

Article

Sodium Dodecyl Sulfate Preferentially Promotes Enclathration of Methane in Mixed Methane-Tetrahydrofuran Hydrates

Asheesh Kumar,[1,3] Rajnish Kumar,[2] and Praveen Linga[1,4,*]

SUMMARY

Methane storage in mixed hydrates is advantageous due to faster kinetics and added stability. However, capacity needs to be improved. Here we study mixed hydrates of methane (CH_4) and tetrahydrofuran (THF), in the presence of sodium dodecyl sulfate (SDS) as a kinetic promoter for hydrate formation. We report the co-existence of pure methane (sI) and mixed CH_4-THF hydrates (sII) in the presence of SDS; however, in the absence of SDS, co-existence of pure THF (sII) and mixed CH_4-THF hydrates (sII) was observed. Thus the presence of SDS preferentially promotes the enclathration of methane over that of THF. Furthermore, through *in situ* Raman spectrometry, complemented by high-pressure differential scanning calorimeter, we present temperature-dependent methane occupancy in small and large cages of sI and sII hydrates. Our findings offer new insights for enhancing the methane storage capacity in more stable sII hydrate configuration for large-scale methane storage via solidified natural gas technology.

INTRODUCTION

Clathrate or gas hydrates are crystalline non-stoichiometric compounds formed by guest molecules, such as CH_4, THF, etc., and host water molecules at a suitable pressure/temperature condition. Depending on the size, composition, and chemical properties of the guest molecules, clathrate hydrates typically crystallize in three different structures, cubic structures I and II (sI and sII) and hexagonal sH. sI and sII hydrates consist of two different types of cages, called small (pentagonal dodecahedron, 5^{12}) and large (tetrakaidecahedron, $5^{12}6^2$ or $5^{12}6^4$) cages. A unit cell of sI hydrate consists of six large $5^{12}6^2$ cages and two small 5^{12} cages formed by 46 water molecules (pure CH_4 hydrate); however, sII hydrate consists of 8 large ($5^{12}6^4$) cages and 16 small (5^{12}) cages formed by 136 water molecules (for example, mixed CH_4-THF hydrate) (Englezos, 1993; Ripmeester et al., 1987; Sloan, 2003; Sloan and Koh, 2007). Recently, we demonstrated that mixed CH_4-THF hydrates (sII) offer a promising approach to scale up the solidified natural gas (SNG) technology by shifting the methane hydrate storage conditions to the milder side while still maintaining very fast hydrate formation kinetics (Veluswamy et al., 2016a, 2016b, 2018). SNG technology provides an excellent opportunity to store natural gas or methane on a large scale (Gudmundsson, 1996; Veluswamy et al., 2018; Wang et al., 2008). Furthermore, to understand the rapid kinetics of mixed hydrate formation, Kumar et al., elucidated the mechanism of mixed CH_4-THF hydrate formation employing high-pressure differential scanning calorimetry (HP μ-DSC); they reported the formation of two types of sII hydrates (pure THF and mixed CH_4-THF hydrates) with a stoichiometric amount of THF (5.56 mol %) in water (Kumar et al., 2016). For pure THF hydrates (THF.17H_2O) the dissociation temperature is 277.5 K at 1.0 bar (THF occupies the large cages and all the small cages are empty), which aids the shifting of mixed CH_4-THF hydrates toward ambient conditions. Furthermore, literature suggests that mixed hydrates of CH_4 and THF (with stoichiometric amount, 5.56 mol % THF) form sII hydrates where all the large cages are occupied by THF and small cages by CH_4 molecules (Seo et al., 2009; Sum et al., 1997; Veluswamy et al., 2018). Seo et al. reported a 36.84% occupancy of small cages by CH_4 and more than 99% occupancy of large cages by THF molecules for mixed CH_4-THF hydrates (Seo et al., 2003). Prasad et al. have also reported that methane did not occupy the large cage for 5.88 mol % THF. At a stoichiometric amount of THF, no C-H stretch from methane was observed in the large cages (Prasad et al., 2009). Thus the relevant literature on CH_4-THF hydrates shows that methane neither occupies the large cages of sII nor co-exists in the resultant hydrate as a mixture of sI and sII hydrates. Higher methane occupancy in small and large cages of sII hydrate (in the presence of THF) would result in a higher methane storage capacity at milder formation conditions. Seo et al. have reported methane occupancy in both the cages (small and large) of sII hydrate, when powdered THF · 17H_2O (formed at 263 K) was exposed to CH_4 gas at a pressure of 5.0 MPa and a temperature of 274 K. They suggested that the occupancy of

[1]Department of Chemical and Biomolecular Engineering, National University of Singapore, Singapore 117 585, Singapore

[2]Department of Chemical Engineering, Indian Institute of Technology Madras, Chennai, India

[3]Present address: Department of Mechanical and Chemical Engineering, The University of Western Australia, Perth, Australia

[4]Lead Contact

*Correspondence: praveen.linga@nus.edu.sg

https://doi.org/10.1016/j.isci.2019.03.020

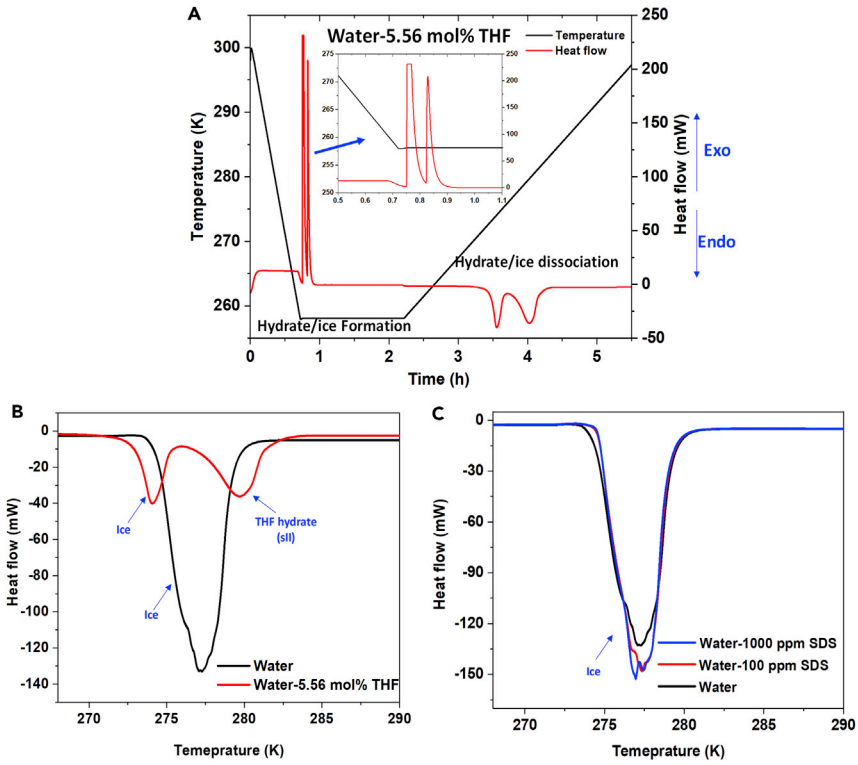

Figure 1. THF Shifts the Ice Melting Peak toward Lower Temperature; Ice Peak Position Is Insensitive to ppm-Level SDS Addition

(A) Typical DSC thermograms for water + 5.56 mol % THF system along with heat flow and temperature profile for ice/hydrate formation and dissociation.

(B and C) (B) Comparison of dissociation thermograms of ice melting and THF hydrate dissociation (water + 5.56 mol % THF). (C) Comparison of dissociation thermograms of ice melting in the presence and absence of SDS (100 and 1,000 ppm) in water.

methane in large cages is kinetically controlled and that it takes a longer time to occupy the large cages (Seo et al., 2009). Thus the presence of kinetic promoters (like sodium dodecyl sulfate [SDS]) and suitable experimental conditions may allow methane to share the large cages with THF and also enhance the small cage occupancy, resulting in a thermodynamically more stable mixed CH_4-THF hydrate. Thus the focus of the present work is to understand the influence of SDS on mixed CH_4-THF hydrate formation at the molecular level and to distinguish the various types of hydrates (pure methane, pure THF, and mixed methane-THF) formed in different thermodynamic or kinetically controlled conditions. In this work, we employ HP μ-DSC and *in situ* Raman spectroscopy to characterize the mixed CH_4-THF hydrates in the presence and absence of SDS. Change in heat flow during hydrate formation and dissociation process in the presence of 5.56 mol % THF (stoichiometric composition) with and without a kinetic promoter (SDS, 100 and 1,000 ppm) was monitored employing HP μ-DSC. The formed hydrates were distinguished using *in situ* Raman spectra in real time. Refer to the Supplemental Information for experimental method and procedures (Figures S1–S3).

RESULTS AND DISCUSSION

Differential Scanning Calorimetric Studies

Effect of THF and SDS in Ice Formation (Without Methane Gas)

In a typical DSC thermogram, upward exothermic peak(s) during cooling step represents hydrate/ice formation, and the endothermic hydrate/ice melting peak(s) can be seen as downward peak(s) during the heating step. Figure 1A shows a typical DSC thermogram for water + 5.56 mol % THF system along with heat flow and temperature profile for ice/hydrate formation and dissociation. The experimental data presented in Figure 1A were obtained at atmospheric pressure. As can be seen in the figure, two exothermic peaks were observed in the cooling step (see inset figure for better clarity), and subsequently, two

endothermic peaks were observed during the heating step. The two exothermic peaks in Figure 1A can be attributed to the formation of ice and sII (pure THF hydrate). Although it is ambiguous to assign the exact peaks to one another, the endothermic peaks can be assigned to ice formation or THF hydrate formation based on the dissociation temperature. To distinguish the ice and THF hydrate melting peaks, we present the heat flow data of dissociation thermogram with respect to temperature for THF hydrate dissociation (water + 5.56 mol % THF) in Figure 1B along with the dissociation thermogram of pure ice dissociation experiment conducted independently (black solid line in Figure 1B). Figure 1B shows two distinct peaks, one for THF hydrate and one for ice (water, which did not participate in the formation of THF hydrate). In addition, we can also see the influence of THF (in the liquid phase) on the melting temperature of ice; the ice melting peak has shifted toward lower temperature (depression in freezing point of ice) when compared with the data presented for pure ice melting. Furthermore, we performed the ice formation experiments with different concentration of SDS in water (100 and 1,000 ppm); Figure 1C compares the dissociation thermograms of ice melting in the presence and absence of SDS in water. We found that the ice melting temperature is insensitive to the addition of SDS in water. Moreover, for better clarity of ice nucleation (or subcooling temperature) in the presence and absence of SDS in water, Figure S4 in Supplemental Information presents the complete ice formation-melting thermograms along with heat flow and temperature profile.

Influence of SDS in Mixed CH_4-THF Hydrate Formation

Figure 2 shows the DSC thermograms for water + 5.56 mol % THF + 100 ppm SDS-CH_4 system along with heat flow and temperature profile for hydrate formation and dissociation (obtained at 6.8 MPa pressure). More precisely, Figure 2A presents two formation-dissociation cycles, which were performed using a temperature ramping program. Run 1 is an isochoric process, in which the temperature was decreased from 303.2 to 263.2 K at 1.0 K/min during hydrate formation step, resulting in an exothermic peak due to hydrate formation; hydrate dissociation during run 1 was ensured by raising the temperature from 263.2 to 308.2 K at 0.10 K/min, resulting in few endothermic and at least one exothermic peak. One quick observation of the thermogram (expanded in Figure 2B) suggests that there is no ice formation during run 1 (only a single exothermic event); however, no ice peak may not mean that all the water got converted into hydrate. On the other hand, for run 2, the temperature was decreased from 308.2 to 258.2 K (lower temperature than that of run 1) during formation path, with rest of the procedure and conditions being the same. Two unique exothermic events (see expanded Figure 2C) are observed during the cooling step (formation step) in run 2, one attributed to ice formation and the other attributed to hydrate formation. The ice formation observed in run 2 is mainly due to higher subcooling leading to a higher driving force for ice nucleation and growth. Hydrate dissociation thermograms as a function of temperature could be compared to distinguish the ice from hydrates; onset of ice dissociation (for run 2) could be seen closer to 273.2 K (refer to Figure 2D). Moreover, Figure 2D represents an unusual dissociation thermogram plotted against temperature; we can see two distinctive endothermic peaks for run 1 and run 2, occurring around 283 and 301 K. These two endothermic peaks suggest the presence of two different structures (sI and sII hydrates) in the resulting solid hydrate phase. The endothermic peak at ~283 K can be attributed to the dissociation of pure CH_4 hydrates (sI), and the endothermic peak at ~ 301 K can be attributed to the dissociation of mixed CH_4-THF hydrates (sII). These peaks are confirmed based on the hydrate phase equilibrium conditions (pressure-temperature curve) available in the literature (Kumar et al., 2018; Nakamura et al., 2003).

Figure 3 presents repeat runs (dissociation thermograms) for water + 5.56 mol % THF + 100 ppm SDS-CH_4 system. On a careful analysis of the dissociation thermogram, it can be observed that in runs 1, 2, and 4, a small dissociation peak of pure THF hydrate is followed by an exothermic peak, signifying hydrate formation event. This exothermic peak represents the formation of mixed hydrate of CH_4-THF (sII); this aspect of methane-water-THF system is explained in detail in our previous works (Kumar et al., 2016, 2019). For the DSC experimental data presented in Figures 2 and 3, the thermodynamic conditions were such that the formation of sI hydrate of methane was possible. The DSC thermogram for water + 5.56 mol % THF-CH_4 system and water-CH_4 system in the absence of SDS is shown in Figure S5. As can be seen in Figure S5, for the water + THF-CH_4 system we do not observe a dissociation peak around 283 K, whereas we can observe a dissociation peak around 301 K. The analysis of the water + THF-CH_4 system in DSC is discussed in more detail in our previous work (Kumar et al., 2016), and the presence of sI hydrates were never observed for the water + THF-CH_4 system. Even earlier literature works report that with a stoichiometric concentration of THF (5.56 mol %), the presence of sI hydrate was not identified (Prasad et al., 2009; Seo et al., 2003). Thus the co-existence of both the structures (sI and sII) observed in Figures 2 and 3 in the

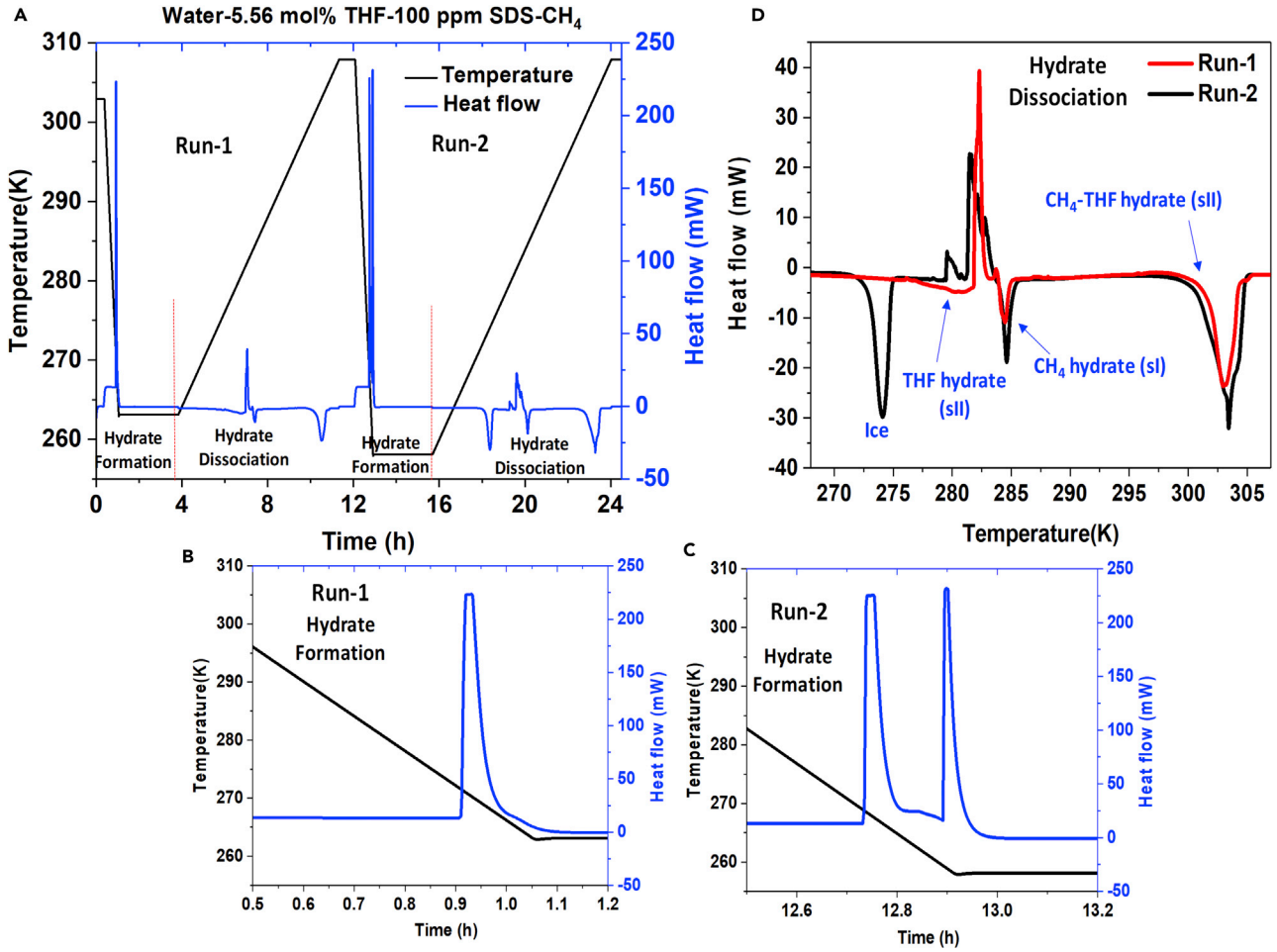

Figure 2. If Thermodynamic Conditions Are Favorable, Co-existence of Pure Methane (sI, structure I) and Mixed CH_4-THF Hydrates (sII, structure II) Could Be Observed in the Presence of SDS

(A) DSC thermograms for water + 5.56 mol % THF +100 ppm SDS-CH_4 system along with heat flow and temperature profile for hydrate formation and dissociation.

(B–D) (B and C) hydrate formation profiles obtained using a temperature ramping program from 303.2 K to 263.2 K and 308.2 K to 258.2 K at 1.0 K/min. (D) Comparison of dissociation thermograms obtained using a temperature ramping program from 263.2 K to 308.2 K and 258.2 K to 308.2 K at 0.10 K/min.

presence of SDS can be attributed to the preferential kinetic promotion of sI hydrate formation; SDS helps in improving the gas diffusion (Kumar et al., 2015) and preferentially enhances the formation of pure methane hydrate (sI). This is an interesting behavior considering that the presence of SDS seems to favor the enclathration of gaseous guest in the resulting mixed hydrate. In Figure S5, a more prominent or significant peak for pure THF hydrate dissociation is observed for water + THF-CH_4 system at around 278 K when SDS is not present in the system. In the presence of SDS (see Figure 2D), pure THF hydrate dissociation is detected for some experiments (a small broader peak seen in run 1 in Figure 2D and runs 1, 2, and 4 in Figure 3), whereas in some experiments (run 2 in Figure 2D and run 3 in Figure 3) it is negligible.

Furthermore, Figure 4 compares the dissociation thermograms obtained for THF (5.56 mol %)-CH_4 and non-THF-CH_4 systems in the presence and absence of SDS (100 and 1,000 ppm). Figure 4A compares the dissociation thermograms for water + 5.56 mol % THF-CH_4 system in the presence and absence of SDS (refer to Figure S6 for repeat runs of 1,000 ppm SDS system). As can be seen in Figure 4A, in the presence of SDS, we see a clear signature of both the structures, sI and sII hydrates; peaks at ~283 and 301 K, respectively, are due to the dissociation of pure methane and mixed CH_4-THF hydrates. In the absence of SDS, (water + 5.56 mol % THF-CH_4 system) no endothermic peak for sI hydrate is observed (can be seen in Figure 4A, black solid line). Furthermore, in the absence of SDS, the formation of pure THF hydrates can be

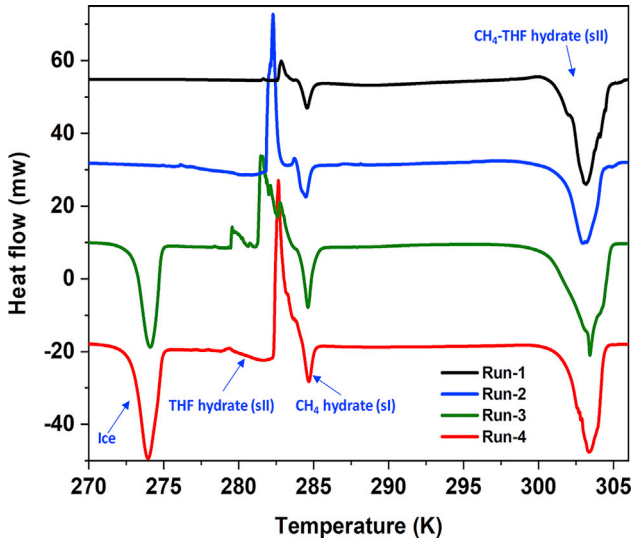

Figure 3. Formation of sI Hydrate in the Presence of 100 ppm SDS Was Repeatable and Consistent

Repeatability of the dissociation thermograms for water + 5.56 mol % THF + 100 ppm SDS-CH_4 system (note: hydrate formation for runs 3 and 4 were obtained using a temperature ramping to 258.2 K and for runs 1 and 2 at 263.2 K).

observed (black curve showing sII hydrates at ~278 K), suggesting lower enclathration of methane in the resultant hydrate. Thus it is evident that SDS preferentially promotes hydrate formation of gaseous species, resulting in the formation of sI hydrate (at suitable thermodynamic condition) or mixed THF-methane hydrate, which maximizes methane storage capacity in the solid hydrate. On the other hand, in the absence of methane, the addition of SDS does not affect the formation kinetics of pure THF hydrate (refer to Figure S7), thus confirming that SDS only enhances enclathration of gaseous species during hydrate growth.

Figure 4B presents the dissociation thermograms of pure CH_4 hydrate in the presence and absence of SDS (water-CH_4 system). Expectedly, we observed only a single endothermic peak (at ~ 283 K) for hydrate dissociation (except ice peak), which corresponds to the dissociation of pure methane hydrates (sI). The addition of SDS to this system was found to enhance the formation of pure methane hydrate (see Figure 4B). Interestingly, in the presence of 1,000 ppm SDS, we observe a huge exothermic peak after the ice dissociation peak (refer to the blue solid line in Figure 4B), which is due to the formation of sI hydrates. A similar peak for sI hydrate growth is observed in the presence of 100 ppm SDS, albeit at a later time, and is of smaller magnitude. This observation suggests that compared with 100 ppm SDS, 1,000 ppm SDS shows better kinetics, resulting in faster enclathration of gaseous species in the solid hydrate (Hayama et al., 2016; Kumar et al., 2015). The SDS-concentration-dependent promotion of hydrate growth is well known in the literature (Kumar et al., 2015).

In Situ Raman Spectroscopic Studies

Raman Measurements at Atmospheric Conditions for Water-THF-SDS Systems

To understand this unusual behavior of SDS for promoting the coexistence of sI and sII hydrates, we performed *in situ* Raman analysis during mixed hydrate formation in an independent experimental facility (Kumar et al., 2019). First, we analyzed the Raman spectra of THF-water system at room temperature conditions (without methane). Figure 5A presents the comparison of Raman spectra obtained for pure THF, water, and water-THF (5.56 mol %), which can be differentiated from each other based on specific stretching frequencies for C-C and C-H stretch of THF and –OH broad band of water (refer to Figure 5A for specific peak positions). Furthermore, to probe the effect of SDS (100 and 1,000 ppm) we compare the Raman spectra obtained at room temperature conditions for pure water and water-THF (5.56 mol %) system in the presence and absence of 100 and 1,000 ppm SDS (Figure 5B). As can be seen in Figure 5B, there is no change in peak positions or no new peaks were observed for SDS (presence of up to 1,000 ppm of SDS does not get detected in bulk solution).

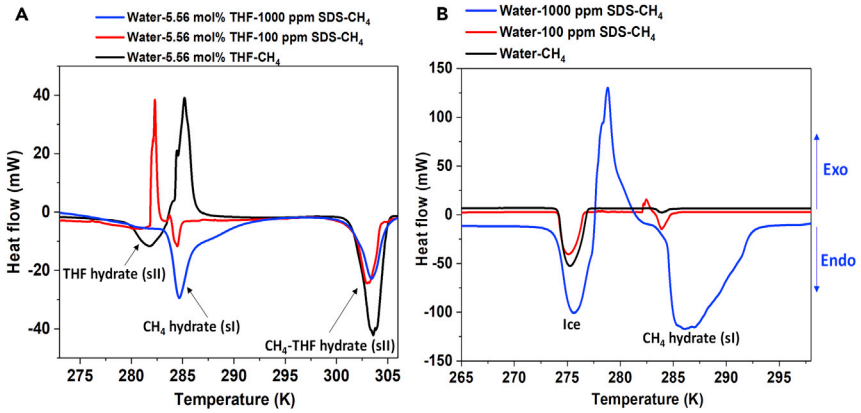

Figure 4. Presence of SDS Improves the Kinetics of Methane Enclathration during Hydrate Growth

(A) Comparison of dissociation thermograms for water-5.56 mol % THF-CH_4 system in the presence and absence of 100 and 1,000 ppm SDS.

(B) Comparison of dissociation thermograms for non-THF systems in the presence and absence of 100 and 1,000 ppm SDS in water.

In Situ Raman Investigations during Pure THF Hydrate Formation

Figure 6 presents the pure THF hydrate formation for water + 5.56 mol % THF + 1,000 ppm SDS system at atmospheric pressure and ~270 K temperature in an unstirred reactor configuration (UTR). Figure 6A presents the pressure and temperature profile during the THF hydrate formation; in the experiment, water and THF mixture is being cooled from 283 K, sharp rise in temperature at 112 minutes corresponds to THF hydrate nucleation. Figure 6B corresponds to Raman spectra taken at different time intervals during THF hydrate formation. THF forms sII hydrate structure (THF·17 H_2O) on its own, in which the THF molecules occupy the large cage and all the small cages are unoccupied or empty (Tulk et al., 1998). As can be seen from Figure 6B a strong split band occurs at ~920 and 892 cm^{-1}, attributing for C–C–C–C stretching vibrations for THF in aqueous phase (0- and 60-min spectra). However, when THF gets entrapped in the large cages of sII hydrate only a single sharp band at ~ 920 cm^{-1} is observed (refer to 140-min spectra). Also, the broad band at 3,100 to 3,600 cm^{-1} corresponding to O–H stretching mode of water in THF solution becomes sharper with hydrate formation (Kumar et al., 2019). The sharp peaks from 2,850 to 3,000 cm^{-1} represent the C–H asymmetric and symmetric stretches of THF (Tulk et al., 1998). Raman spectra and pressure-temperature profile for water + 5.56 mol % THF and water +5.56 mol % THF + 100 ppm SDS systems have been presented in the Supplemental Information, Figures S8 and S9, respectively. We did not observe any significant spectral change during pure THF hydrate formation in the presence and absence of SDS.

In Situ Raman Investigations during Mixed CH_4-THF Hydrate Formation

Furthermore, to understand the coexistence of sI (pure methane) and sII hydrates (mixed CH_4-THF hydrate), we performed *in situ* Raman analysis during the hydrate formation. As discussed in procedure #1, the experiments were performed in various steps; Figure 7A presents the pressure-temperature profile of an experiment conducted in a UTR configuration using 5.56 mol % THF and 1,000 ppm SDS in which pure THF hydrate was formed first at 268 K temperature and atmospheric pressure (step A) and thereafter methane gas was injected (step B) into the pre-formed THF hydrates. Steps C and D represent the temperature rise to 275 and 283 K, respectively (Figure 7A); this was essentially done to study the dissociation behavior of the resultant hydrate. Figure 7B presents the corresponding Raman spectra obtained during these different steps. Pure THF hydrate formation (step A) has already been discussed in detail in Figure 6. Furthermore, step B in Figure 7A presents the pressure and temperature profile during the insertion of methane (at 7.0 MPa and ~268 K temperature) into the pure THF hydrates, and the black curve in Figure 7B shows the corresponding Raman spectra for this step. The peak at ~ 920 cm^{-1} (refer to Figure 7B, black curve) corresponds to the occupancy of THF in the large cages of sII hydrate, which is consistent with that described in Figure 6. However, two extra characteristic Raman bands were observed in the C-H stretching region (refer to inset Figure 7C for better clarity); band at 2,914 cm^{-1} may correspond to the C-H stretching of methane in 5^{12} cages (small), and band at ~2,904 cm^{-1} corresponds to the C-H stretching of methane in $5^{12}6^2$ or $5^{12}6^4$ cages (large) of sI or sII hydrates (Sum et al., 1997). The C-H stretch of methane

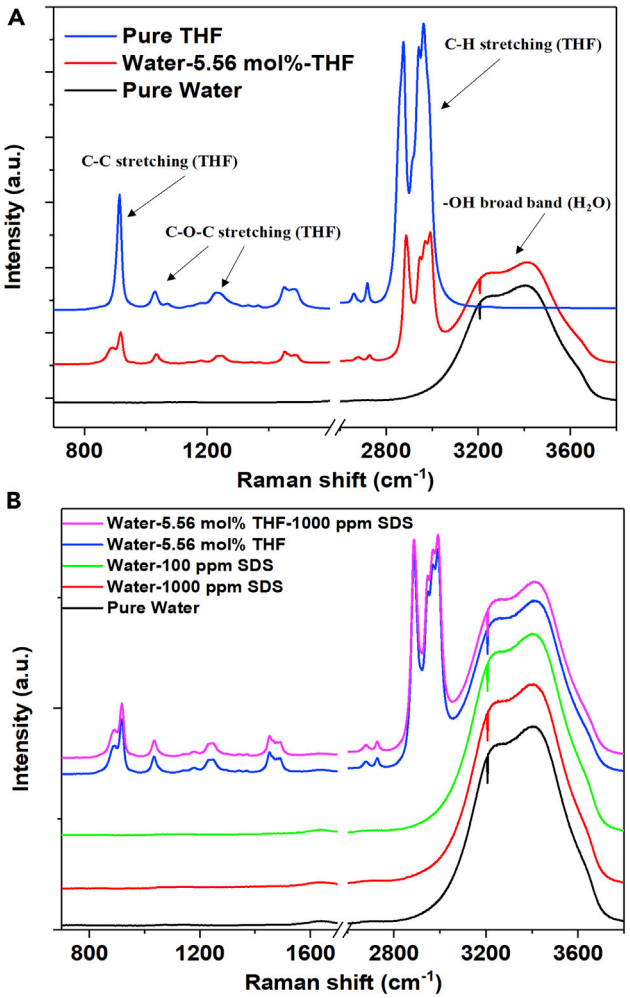

Figure 5. Raman Analysis of Different Systems at Room Temperature and Atmospheric Pressure

(A) Comparison of Raman spectra obtained at room temperature conditions for pure THF, water, and water-THF (5.56 mol %) system.

(B) Comparison of Raman spectra obtained at room temperature conditions for pure water and water-THF (5.56 mol %) system in the presence and absence of 100 and 1,000 ppm SDS.

in $5^{12}6^4$ cages (large) of sII hydrates occurs at ~2,903 cm^{-1}, and that in $5^{12}6^2$ cages (large) of sI hydrates occurs at 2,904 cm^{-1}; similarly the C-H stretch of methane in 5^{12} cages (small) of sII hydrates occurs at 2,913.7 cm^{-1}, and that in sI hydrates occurs at 2,915 cm^{-1} (Sum et al., 1997).

In this work, the experiment for Raman analysis was designed in such a way that in step A, pure sII hydrate forms through the incorporation of THF in the large sII cages, and in step B, methane gas is incorporated. Two scenarios exist; in the first scenario all the THF in liquid solution is consumed for the formation of sII hydrate, and methane, which is supplied in step B, only occupies the small cages. In this scenario, we should get only one peak for methane from the small cages of resultant sII hydrate. However, a split peak as observed in this study points to a more complex scenario. In the second scenario, in step B, when the system is exposed to methane, a new equilibrium is achieved. In this new equilibrium, after step B, methane shares the large cages with THF in sII configuration, and if the temperature and pressure are favorable, sI hydrate may additionally be formed, where both large and small cages are occupied by methane alone. Unfortunately, methane peak positions are such that the extent of sI/sII hydrate formation cannot be confirmed by Raman spectroscopy alone. It is difficult to say whether this band at 2,904 cm^{-1} corresponds to the large cage of sI hydrate or sII hydrates, but it is proved beyond any doubt that in the presence of SDS, methane also occupies the large cages in the resulting hydrate structure, thus enhancing the storage capacity.

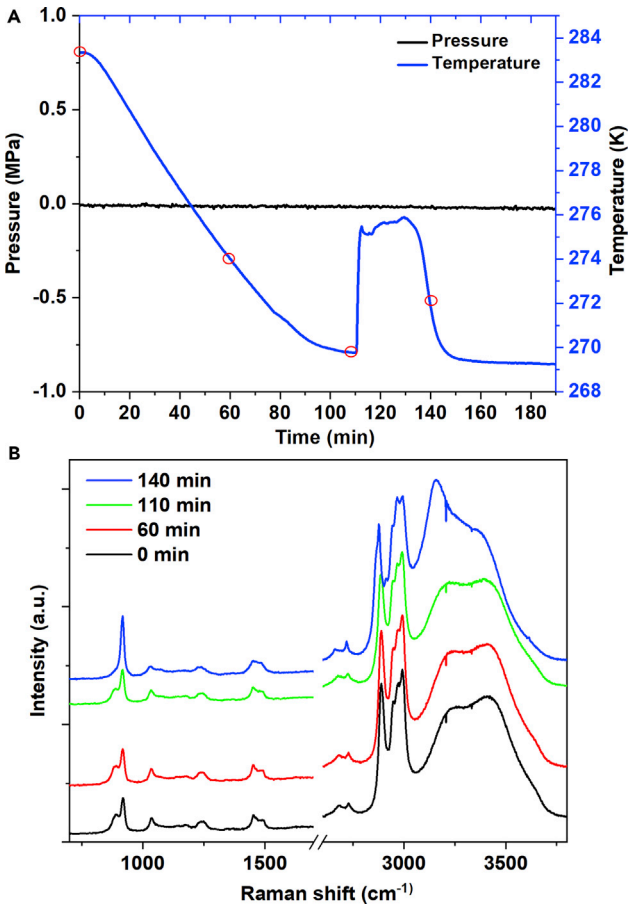

Figure 6. *In Situ* Raman Measurements during Pure THF Hydrate Formation

Pure THF hydrate formation for water + 5.56 mol % THF + 1,000 ppm SDS system at atmospheric pressure and ~270 K temperature in an unstirred reactor configuration.

(A and B) (A) Pressure and temperature profile during the THF hydrate formation. (B) Corresponding Raman spectra taken at a different time interval during THF hydrate formation.

Analyzing the results further, when temperature increases to 275 K (step C), there is a marginal drop in pressure (~7 MPa) (refer to the zoomed section of Figure 7A), which signifies further hydrate growth. However, the two peaks from methane in large and small cages remain unchanged signifying equal distribution of additional methane in small and large cages (refer to Figure 7C). Pure THF hydrates are stable at these conditions, which makes this step mass transfer limited for further mixed CH_4-THF hydrate formation and growth (Zhong et al., 2017).

In step D, the temperature was increased to 283.2 K; at this temperature pure sII THF hydrate is unstable (at ~278 K, THF hydrate starts to dissociate). However, formation and growth of mixed THF-CH_4 hydrate are still possible, which results in rapid pressure drop and sharp temperature spike due to enclathration of methane molecule in the small cages of mixed CH_4-THF hydrates (sII). This is an interesting observation; the degree of bond alteration is quite significant at this stage, which results in net heat release. After step D, no peak for methane in the large cages was observed at 283.2 K (refer to Figure 7C). Owing to thermodynamic limitation it seems the system went to a new equilibrium where most of the large cages are occupied by THF and all the small cages are occupied by methane. Similar experiments (with few modifications) with or without SDS were performed with the water-THF solution. These are included in Supplemental Information Figures S10 and S11.

Furthermore, we performed an additional experiment as per procedure #2 (discussed in the experimental section) in a UTR configuration using 5.56 mol % THF and 100 ppm SDS at 7.5 MPa. Procedure #2 basically replicates the experiments done on DSC. Pressure-temperature profile for this experiment along with

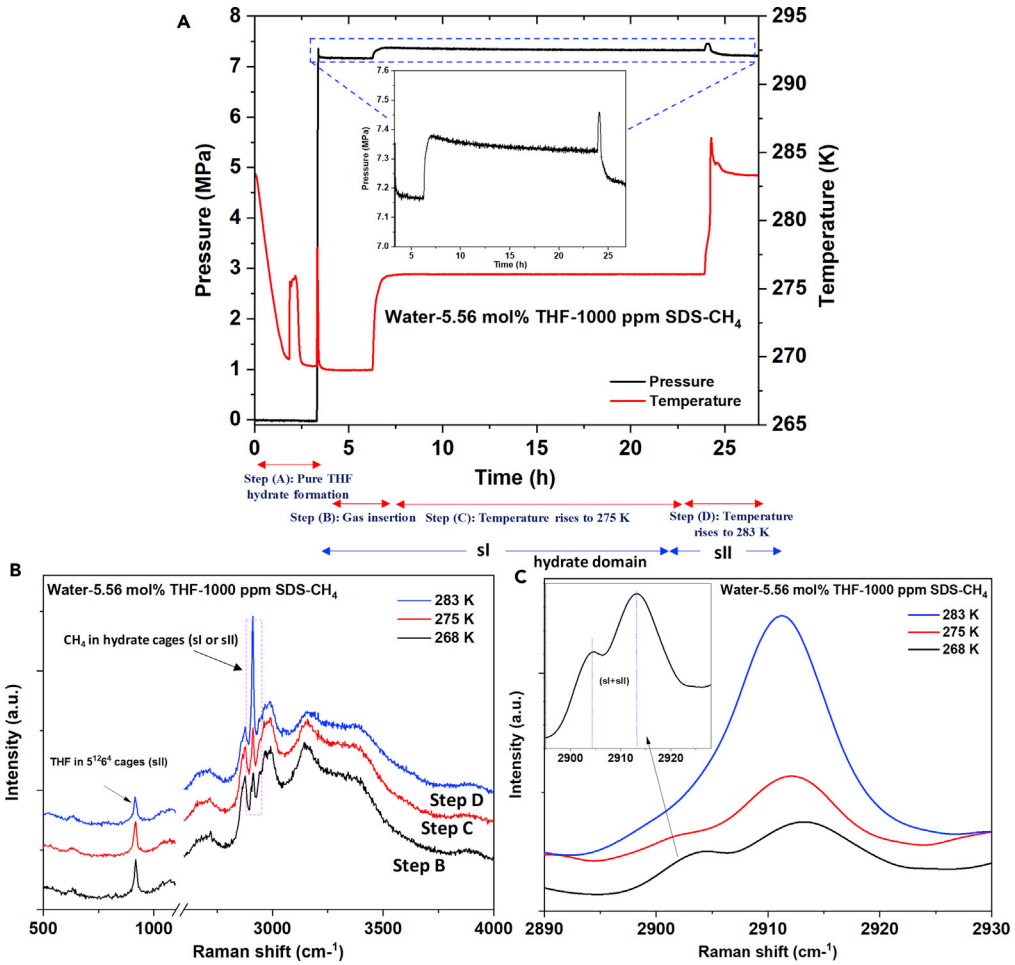

Figure 7. *In Situ* Raman Measurements during Mixed CH_4-THF Hydrate Formation (Procedure #1)

(A) Pressure-temperature profile of an experiment conducted in a UTR configuration using 5.56 mol % THF and 1,000 ppm SDS. (B) Raman spectra (full spectral range) obtained for different steps (step B–D). (C) Raman spectra (C–H stretching region) obtained for different steps at 268, 275 and 283 K; inset presents the specific peaks for the occupancy of methane in small (2,914 cm^{-1}) and large cages (2,904 cm^{-1}). (Refer to procedure#1, experimental section.)

Raman spectra has been presented in Figure 8. As can be seen in Figure 8A, the pressure immediately starts to drop after gas injection in a precooled reactor due to hydrate formation and cooling effect. Furthermore, as can be seen in Figure 8B, through the Raman spectra, we observe that both the cages (small and large) are present (refer to Figures 8C and 8D for peaks corresponding to methane occupancy in small and large cages). Interestingly, Raman band at 2,915 cm^{-1} (Figure 8C, 5 min) is most prominent, which corresponds to the C-H stretching of methane in 5^{12} cages (small) of sI hydrate. Upon annealing, the peak at 2,915 cm^{-1} shift to 2,913 cm^{-1} and the band at 2,904 cm^{-1} (5 min) corresponding to the C-H stretching of methane in $5^{12}6^2$ cages (large) disappears (refer to 100-min spectra in Figure 8C). These observations can be attributed to the structural transformation of kinetically favorable pure methane sI hydrate to thermodynamically favorable mixed CH_4-THF sII hydrates (Sum et al., 1997). This observation clearly shows that under optimal condition, in the presence of SDS, a more stable form of mixed CH_4-THF hydrate could be formed in which methane can share the large cages with THF and also occupy the small cages in larger numbers. Similar to Figure 8, an experiment was conducted in the absence of SDS (water + 5.56 mol % THF-CH_4) and presented in Supplemental Information Figure S12; the assignment of the bands obtained for Figure S12 is consistent with that described for Figure 8.

In summary, we employed HP μ-DSC and *in situ* Raman spectroscopy to investigate the effect of SDS (100 and 1,000 ppm) on mixed CH_4-THF hydrate formation. It was observed that even 100 ppm

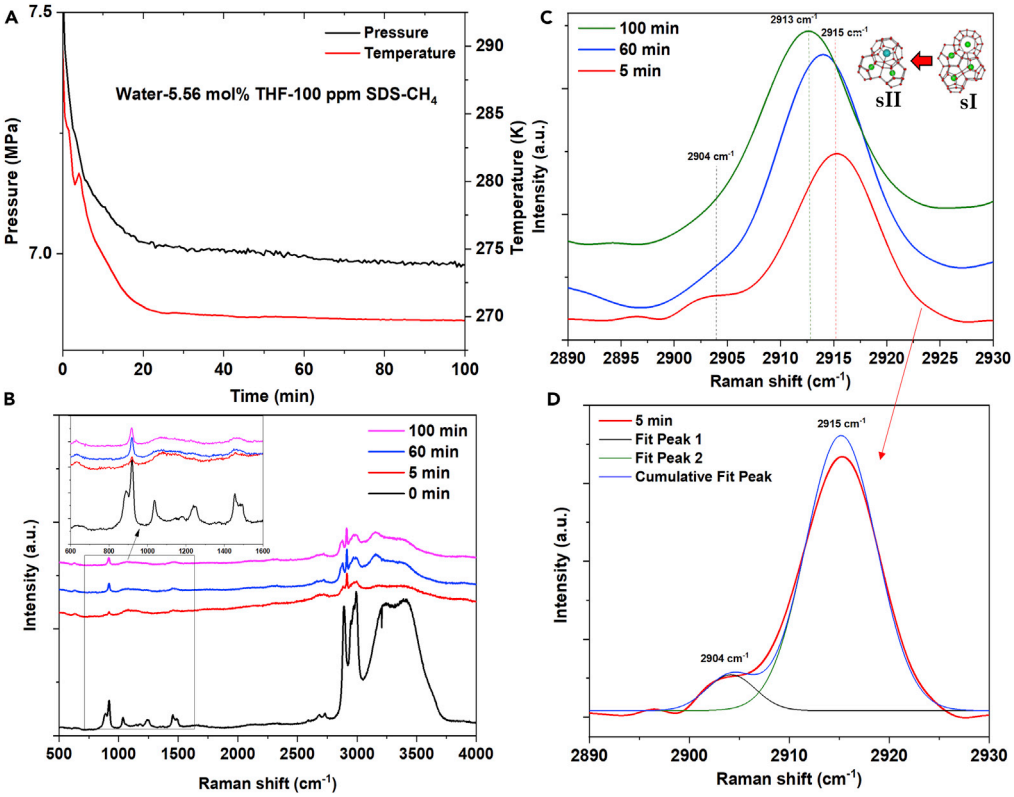

Figure 8. *In Situ* Raman Measurements during Mixed CH_4-THF Hydrate Formation (Procedure#2)

(A and B) (A) Pressure-temperature profile of an experiment conducted in a UTR configuration (precooled at 268 K) using 5.56 mol % THF and 100 ppm SDS at 7.5 MPa. (B) Raman spectra (full spectral range) obtained for different steps at different time intervals.

(C) Specific peaks for the occupancy of methane in small (2,914 cm^{-1}) and large cages (2,904 cm^{-1}).

(D) Peak fitting to distinguish the small and large cage peaks. (Refer to procedure #2, experimental section.)

SDS in a water-THF solution improves the kinetics significantly. The presence of SDS improves the nucleation and growth of sI hydrate (pure methane hydrates) crystals. Furthermore, if the formation of sI hydrate is not possible due to thermodynamic limitations, the presence of SDS in the water-THF system may promote formation of mixed CH_4-THF (sII) hydrate with significantly higher methane to THF ratio. Experimental observation suggests that the formation of mixed CH_4-THF hydrate in the presence of SDS could potentially enhance the storage capacity by allowing methane to share the large cages with THF and enhancing methane occupancy in the small cages of the resultant sII hydrate.

Limitations of the Study

There are few concerns remaining to be addressed with regard to structure elucidation and cage occupancy (quantitatively). *In situ* powder X-ray diffraction (PXRD) and nuclear magnetic resonance measurements could shed further quantitative insights on the structure elucidation and cage occupancy by following the integrated intensity of methane molecules occupying hydrate cages in structure I or II.

METHODS

All methods can be found in the accompanying Transparent Methods supplemental file.

SUPPLEMENTAL INFORMATION

Supplemental Information can be found online at https://doi.org/10.1016/j.isci.2019.03.020.

ACKNOWLEDGMENTS

The work was funded in part under the Energy Innovation Research Programme (EIRP, Award No. NRF2015EWTEIRP002-002), administrated by the Energy Market Authority (EMA), and funded by the National Research Foundation (NRF), Singapore.

AUTHOR CONTRIBUTIONS

P.L., A.K., and R.K. designed and formulated the experimental work plan. A.K. performed all the experiments. R.K. is an expert in Raman analysis and reviewed the discussion pertaining to the characterization. R.K. and P.L. reviewed and revised the manuscript. All authors read and approved the manuscript before submission.

DECLARATION OF INTERESTS

The authors declare no competing interests.

Received: January 5, 2019
Revised: March 5, 2019
Accepted: March 19, 2019
Published: April 26, 2019

REFERENCES

Englezos, P. (1993). Clathrate hydrates. Ind. Eng. Chem. Res. *32*, 1251–1274.

Gudmundsson, J.S. (1996). Method for production of gas hydrates for transportation and storage (Google Patents).

Hayama, H., Mitarai, M., Mori, H., Verrett, J., Servio, P., and Ohmura, R. (2016). Surfactant effects on crystal growth dynamics and crystal morphology of methane hydrate formed at gas/liquid interface. Cryst. Growth Des. *16*, 6084–6088.

Kumar, A., Bhattacharjee, G., Kulkarni, B.D., and Kumar, R. (2015). Role of surfactants in promoting gas hydrate formation. Ind. Eng. Chem. Res. *54*, 12217–12232.

Kumar, A., Daraboina, N., Kumar, R., and Linga, P. (2016). Experimental investigation to elucidate why tetrahydrofuran rapidly promotes methane hydrate formation kinetics: applicable to energy storage. J. Phys. Chem. C *120*, 29062–29068.

Kumar, A., Vedula, S.S., Kumar, R., and Linga, P. (2018). Hydrate phase equilibrium data of mixed methane-tetrahydrofuran hydrates in saline water. J. Chem. Thermodyn. *117*, 2–8.

Kumar, A., Veluswamy, H.P., Linga, P., and Kumar, R. (2019). Molecular level investigations and stability analysis of mixed methane-tetrahydrofuran hydrates: implications to energy storage. Fuel *236*, 1505–1511.

Nakamura, T., Makino, T., Sugahara, T., and Ohgaki, K. (2003). Stability boundaries of gas hydrates helped by methane—structure-H hydrates of methylcyclohexane and cis-1,2-dimethylcyclohexane. Chem. Eng. Sci. *58*, 269–273.

Prasad, P.S.R., Sowjanya, Y., and Shiva Prasad, K. (2009). Micro-Raman investigations of mixed gas hydrates. Vibrational Spectrosc. *50*, 319–323.

Ripmeester, J.A., Tse, J.S., Ratcliffe, C.I., and Powell, B.M. (1987). A new clathrate hydrate structure. Nature *325*, 135–136.

Seo, Y.-T., Lee, H., Moudrakovski, I., and Ripmeester, J.A. (2003). Phase Behavior and structural characterization of coexisting pure and mixed clathrate hydrates. ChemPhysChem *4*, 379–382.

Seo, Y., Lee, J.-W., Kumar, R., Moudrakovski, I.L., Lee, H., and Ripmeester, J.A. (2009). Tuning the composition of guest molecules in clathrate hydrates: NMR identification and its significance to gas storage. Chem. Asian J. *4*, 1266–1274.

Sloan, E.D. (2003). Fundamental principles and applications of natural gas hydrates. Nature *426*, 353–363.

Sloan, E.D., and Koh, C.A. (2007). Clathrate Hydrates of Natural Gases (CRC Press).

Sum, A.K., Burruss, R.C., and Sloan, E.D. (1997). Measurement of clathrate hydrates via Raman spectroscopy. J. Phys. Chem. B *101*, 7371–7377.

Tulk, C.A., Klug, D.D., and Ripmeester, J.A. (1998). Raman Spectroscopic studies of THF clathrate hydrate. J. Phys. Chem. A *102*, 8734–8739.

Veluswamy, H.P., Kumar, A., Seo, Y., Lee, J.D., and Linga, P. (2018). A review of solidified natural gas (SNG) technology for gas storage via clathrate hydrates. Appl. Energy *216*, 262–285.

Veluswamy, H.P., Kumar, S., Kumar, R., Rangsunvigit, P., and Linga, P. (2016a). Enhanced clathrate hydrate formation kinetics at near ambient temperatures and moderate pressures: application to natural gas storage. Fuel *182*, 907–919.

Veluswamy, H.P., Wong, A.J.H., Babu, P., Kumar, R., Kulprathipanja, S., Rangsunvigit, P., and Linga, P. (2016b). Rapid methane hydrate formation to develop a cost effective large scale energy storage system. Chem. Eng. J. *290*, 161–173.

Wang, W., Bray, C.L., Adams, D.J., and Cooper, A.I. (2008). Methane storage in dry water gas hydrates. J. Am. Chem. Soc. *130*, 11608–11609.

Zhong, J.-R., Chen, L.-T., Liu, T.-C., Zeng, X.-Y., Sun, Y.-F., Sun, C.-Y., Liu, B., Chen, G.-J., and Ripmeester, J.A. (2017). Sieving of hydrogen-containing gas mixtures with tetrahydrofuran hydrate. J. Phys. Chem. C *121*, 27822–27829.

ISCI, Volume *14*

Supplemental Information

Sodium Dodecyl Sulfate Preferentially Promotes Enclathration of Methane in Mixed Methane-Tetrahydrofuran Hydrates

Asheesh Kumar, Rajnish Kumar, and Praveen Linga

Supplemental Information

TRANSPARENT METHODS

Materials

Methane gas with the purity of 99.9% was procured from Singapore Oxygen Air Liquide Private Ltd (SOXAL). Tetrahydrofuran (THF) of 99.99% purity and sodium dodecyl sulfate (SDS) of biotechnology grade (99% pure) were purchased from Fisher Chemicals and AMRESCO respectively. De-ionized water was used in all the experiments.

Experimental Apparatus

High-pressure micro-differential scanning calorimeter

Supplemental Figure S1 presents the schematic diagram of the experimental setup. A high-pressure differential scanning calorimeter (HP μ-DSC7 Evo, Setaram Inc.) was used in the present work. The details of the high-pressure calorimetry is described elsewhere in the literature (Kumar et al., 2016; Kumar et al., 2018; Le Parlouër et al., 2004). Briefly, the HP μ-DSC can be used for a temperature ranges from -45°C (228.15K) up to 120°C (393.15K) and a pressure of up to 400 bars (40 MPa). The HP μ-DSC has a resolution of 0.02 μW and a temperature deviation of ±0.2 K.

In-situ Raman spectroscopy coupled with high-pressure reactor

The schematic diagram of the experimental setup is presented in Figure S2 (Kumar et al., 2019a), which consists of a high-pressure crystallizer (6.0 cm ID and 8.0 cm height) enclosed with a cooling jacket which is connected to the external refrigerator (Polyscience) to maintain the crystallizer content at experimental temperature. One pressure transducer (Rosemount) and thermocouple (omega, T-type) were coupled to the crystallizer to measure the real time pressure and temperature respectively. Both the pressure transmitter and thermocouple are connected to a Data Acquisition (DAQ) system (National Instruments) which is connected to a computer (PC).

Temperature and pressure data were recorded every 30s, using a LabVIEW software (National Instruments). The reactor was also coupled with the Raman probe, which provides the *in-situ* Raman spectrum. Location of the Raman probe has also been presented in the schematic diagram; more precisely, there are three ports in the crystallizer for Raman probe, one can be used to focus the laser in the gas phase and other two for liquid phase at different location (at 1 and 2 cm height from bottom end).

Specifically, a dispersive laser Raman Spectrometer (Model: SRaman-532) is employed for *in-situ* characterization of mixed CH_4-THF hydrates. More detail of the similar spectrometer is available in literature (Hong et al., 2012; Kumar et al., 2019b; Lee et al., 2015). This spectrometer is coupled with the crystallizer through a probe which consist of two optical fibers, one of them transmits the laser (wavelength of 532 nm with a laser power of 42 mW) inside the crystallizer and other transfer the signals to the spectrometer. The wide spectral coverage is 150-4490 cm^{-1} with a resolution of 2.8 cm^{-1}/pixel at 2200 cm^{-1}. The Raman spectra obtained during hydrate formation was with the integration time of 1.0 sec (frames averaged per measurement:10) and with an interval time of 30 sec.

Experimental Procedures

Procedure used for HP µ-DSC measurements

150 µl of water/THF/SDS solution was charged to the DSC sample cell. The solution in the sample cell was purged with the methane gas at least three times to remove any residual air. Later, the sample cell was pressurized with methane to the desired pressure and a well-established method of isothermal temperature program was used for hydrate nucleation and growth in all the experiments (Daraboina et al., 2013; Daraboina et al., 2011; Davies et al., 2009). In this method, the temperature was dropped from 298.2K to 263.2 K at the rate of 1 K/min and kept constant at

263.2 K until hydrate formation event is confirmed through an exothermic peak, representing hydrate nucleation and growth. After completion of hydrate formation (~4-5h), the temperature was gradually raised to 308.2 K at the rate of 0.10 K/min to observe hydrate dissociation as onset of endothermic peaks. Some experiments were performed by dropping temperature from 308.2K to 258.2 K at the rate of 1 K/min for hydrate formation (to confirm the ice peak) and dissociation by rising temperature from 258.2 K to 308.2 K at 0.10 K/min.

Procedure used for *in-situ* Raman measurements

Experiments with Raman measurements were started using the procedure as described for DSC measurements, the test solution was cooled from 298.2K to 268.2K in an unstirred reactor configuration (UTR) at experimental pressure (~7.2 MPa). Possibility of sI hydrate formation from pure methane exist at lower temperature, however, no Raman signature for sI hydrates was observed. Further experiments were done with a modified procedure adopted from our previous work (Kumar et al., 2016; Seo et al., 2009).

Raman measurements procedure I: Flow sheet of the experimental procedure used for *in-situ* Raman measurements is presented in Figure S3. All the experiments were performed in an UTR in batch mode. As can be seen in the flow sheet, the reactor or crystallizer was filled with the required volume of 5.56 mol% THF-water/SDS solution (32.4 ml solution [25.6 ml water+6.8 ml THF] which allows the Raman probe-1 in the solution, close to the gas-liquid interface). Raman measurements were performed in multiple steps at various temperature conditions. In the first step (step A), the crystallizer content were cooled to 270 K at atmospheric pressure, resulting in pure THF hydrates. After the formation of THF hydrates, crystallizer was pressurized with the methane gas to the required experimental pressure of ~7.2 MPa at 270 K (step B) and simultaneously, real time Raman spectrometer started to record the Raman spectra, every 30 sec. In step C, temperature

was increased to the 275K to ensure the melting of ice (if any) and further enhancement in water to hydrate conversion. Finally, in step (D), temperature was increased to 283K to dissociate the THF hydrate and perhaps to form mixed CH_4-THF hydrate. Temperature and pressure data were recorded at every 30-second intervals using DAQ system and *in-situ* Raman measurements were continued in all the steps. After completion of hydrate formation step, the formed hydrate was dissociated by depressurization to 1.0 MPa and increasing the temperature to 300K(Veluswamy et al., 2017).

Raman measurement procedure II: Further, to simulate the DSC procedure, we inserted the test solution containing Water + THF + SDS in a precooled reactor (268.2 K) and pressurized the reactor with methane at the experimental pressure, *in-situ* Raman measurements were continued throughout the operation.

SUPPLEMENTAL FIGURES

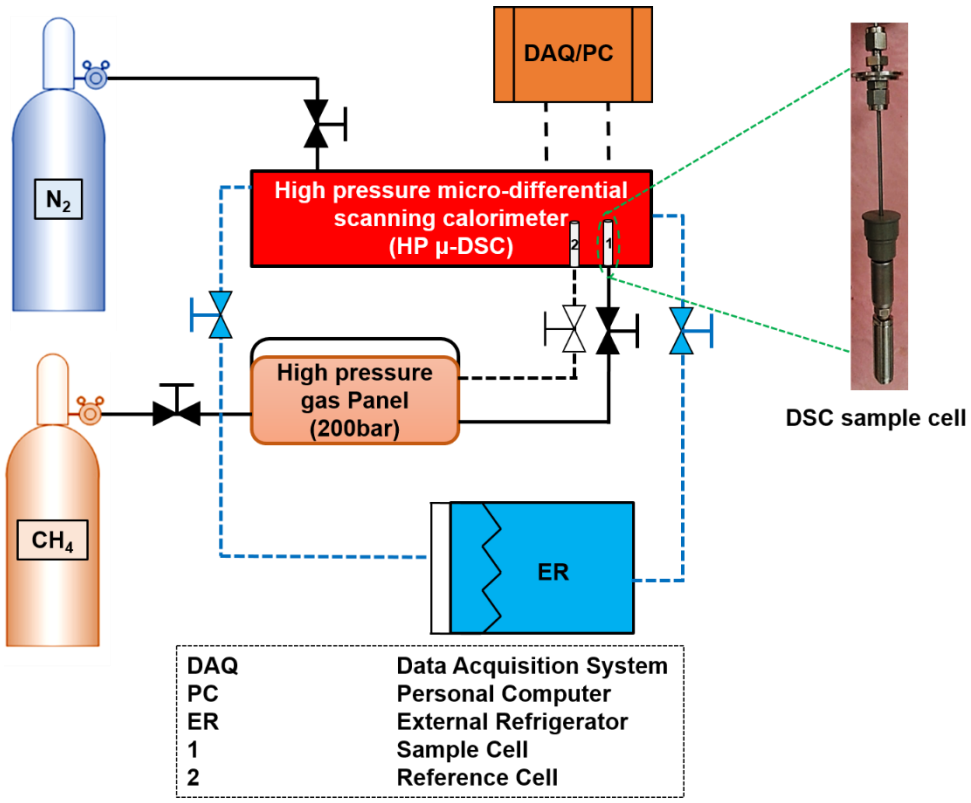

Figure S1. Schematic diagram of experimental setup (High-pressure micro-differential scanning calorimeter) adopted from our previous paper (Kumar et al., 2016).

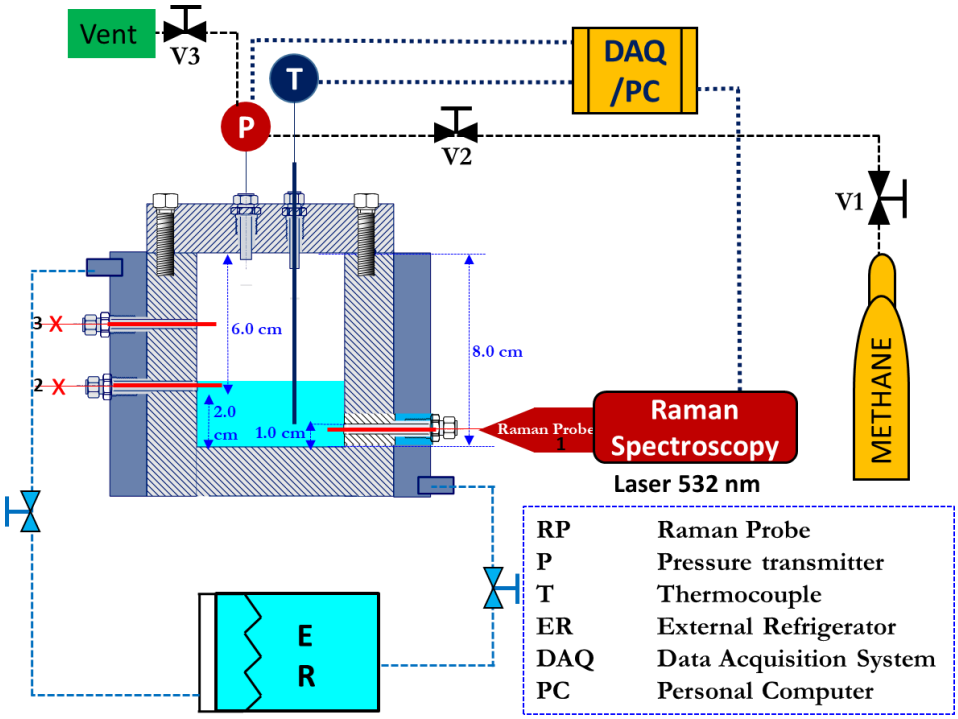

Figure S2. Schematic diagram of experimental setup employed for Raman measurements (*in-situ* Raman setup coupled with high-pressure SS-reactor)

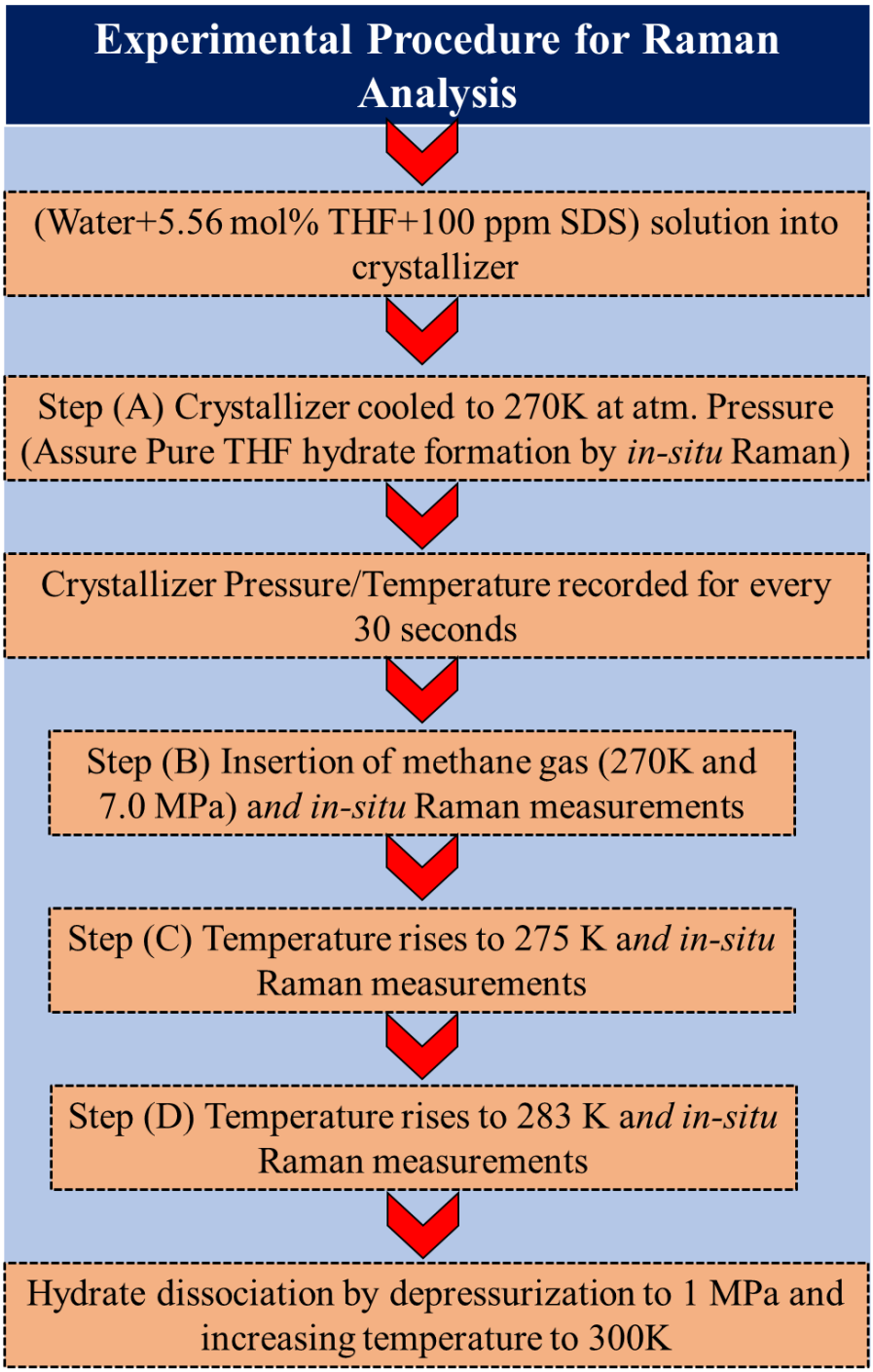

Figure S3. Flow sheet of the experimental procedure I used for *in-situ* Raman measurements

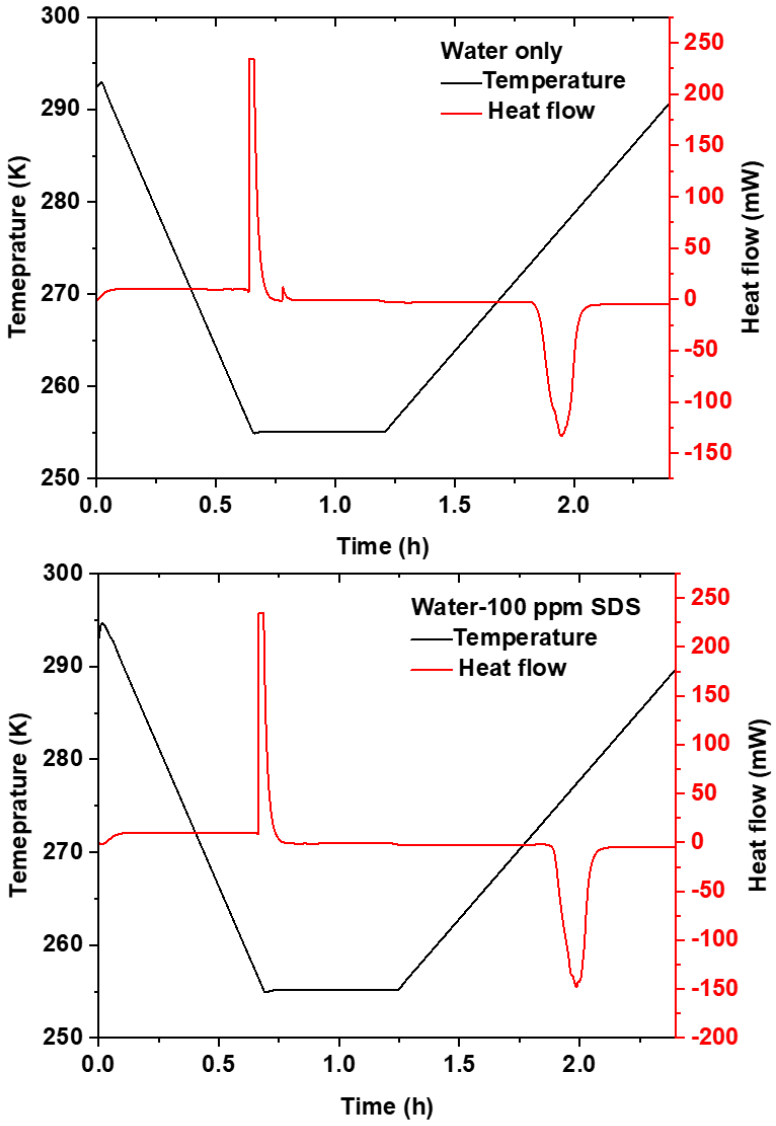

Figure S4. Typical DSC thermograms for Water and water-100 ppm SDS system along with heat flow and temperature profile for ice formation and decomposition. Related to the effect of THF and SDS in ice formation (without methane gas) section in results and discussion.

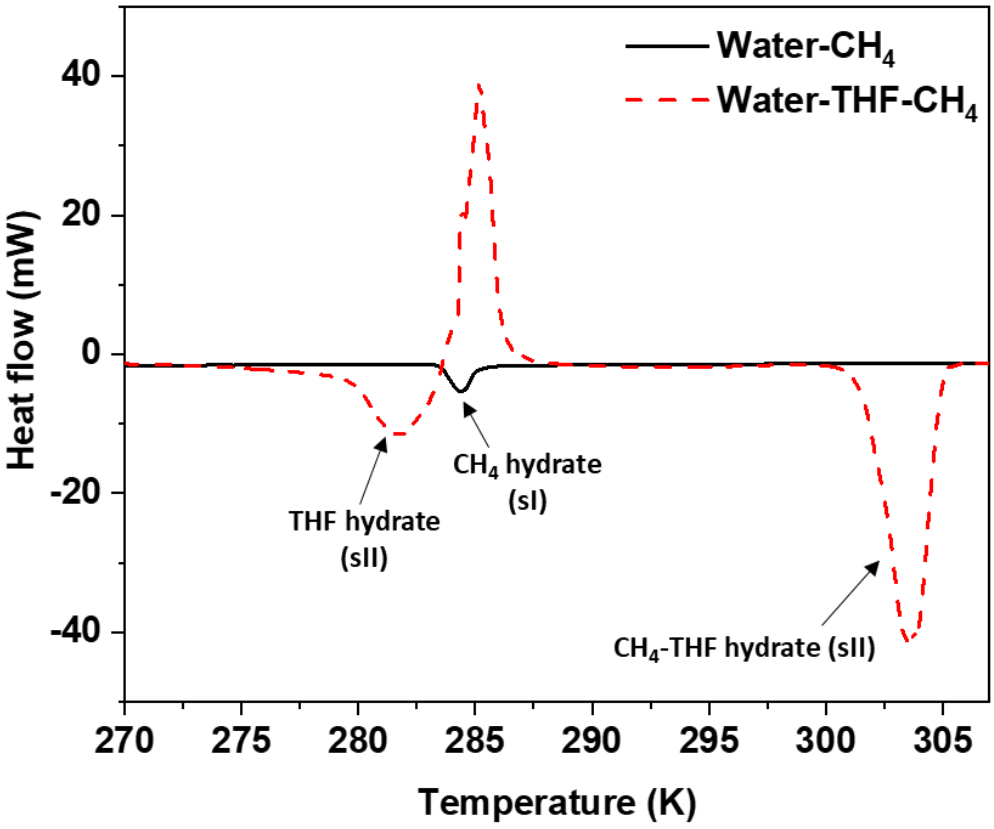

Figure S5. Comparison of dissociation thermograms for Water+5.56 mol% THF system and non THF system obtained at a constant methane gas pressure of 6.8 MPa. Related to the influence of SDS in mixed CH_4-THF hydrate formation section (Figure 2 and 3 discussion) in results and discussion.

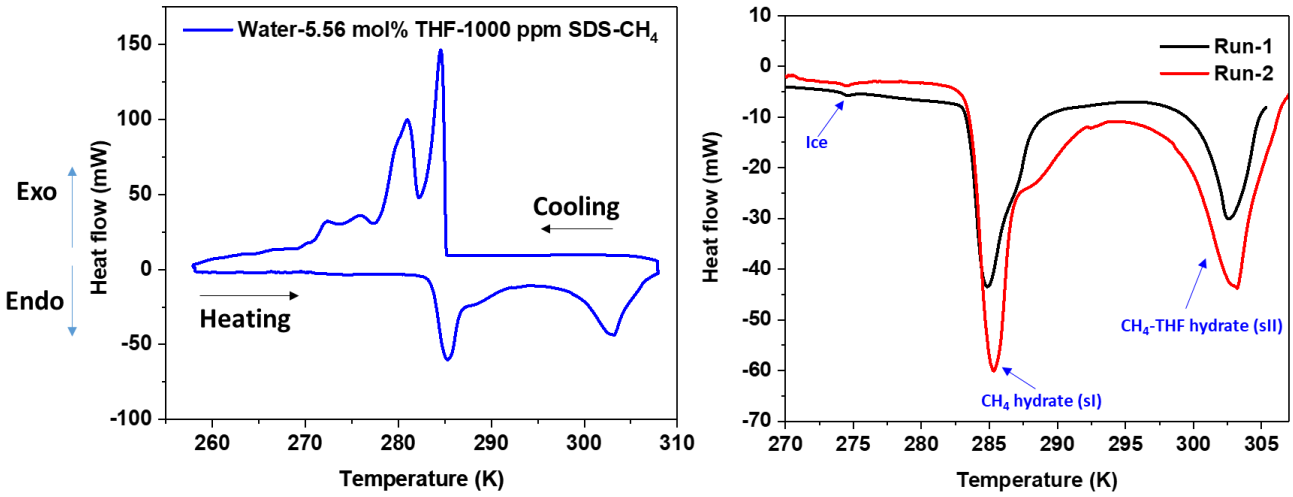

Figure S6. Independent repeat runs (Dissociation thermograms) along with hydrate formation-dissociation cycle for Water-5.56 mol% THF-1000ppm SDS-CH_4 system. Related to Figure 4 discussion in results and discussion section.

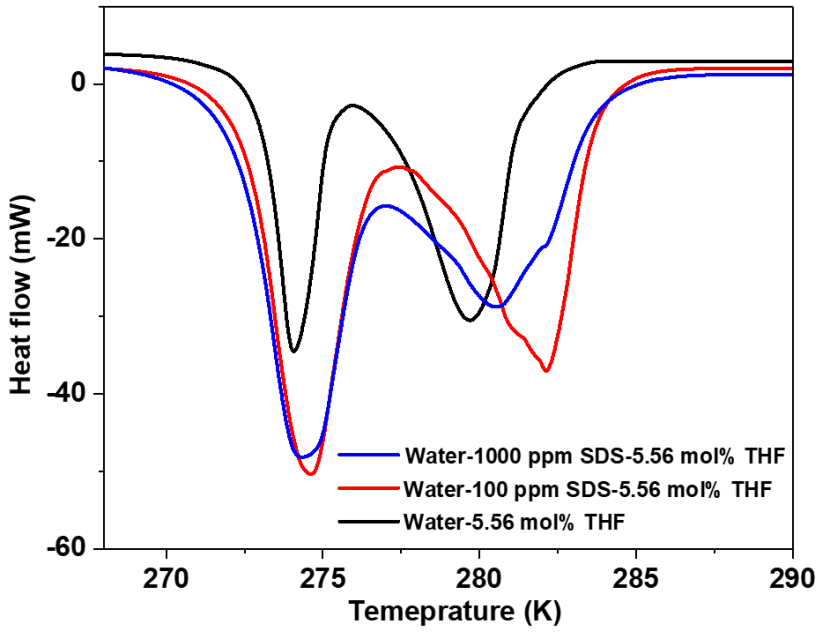

Figure S7. Comparison of dissociation thermograms for Water-5.56 mol% THF system in absence /presence (100/1000 ppm) SDS obtained at atmospheric pressure (no methane). Related to Figure 4 discussion in results and discussion section.

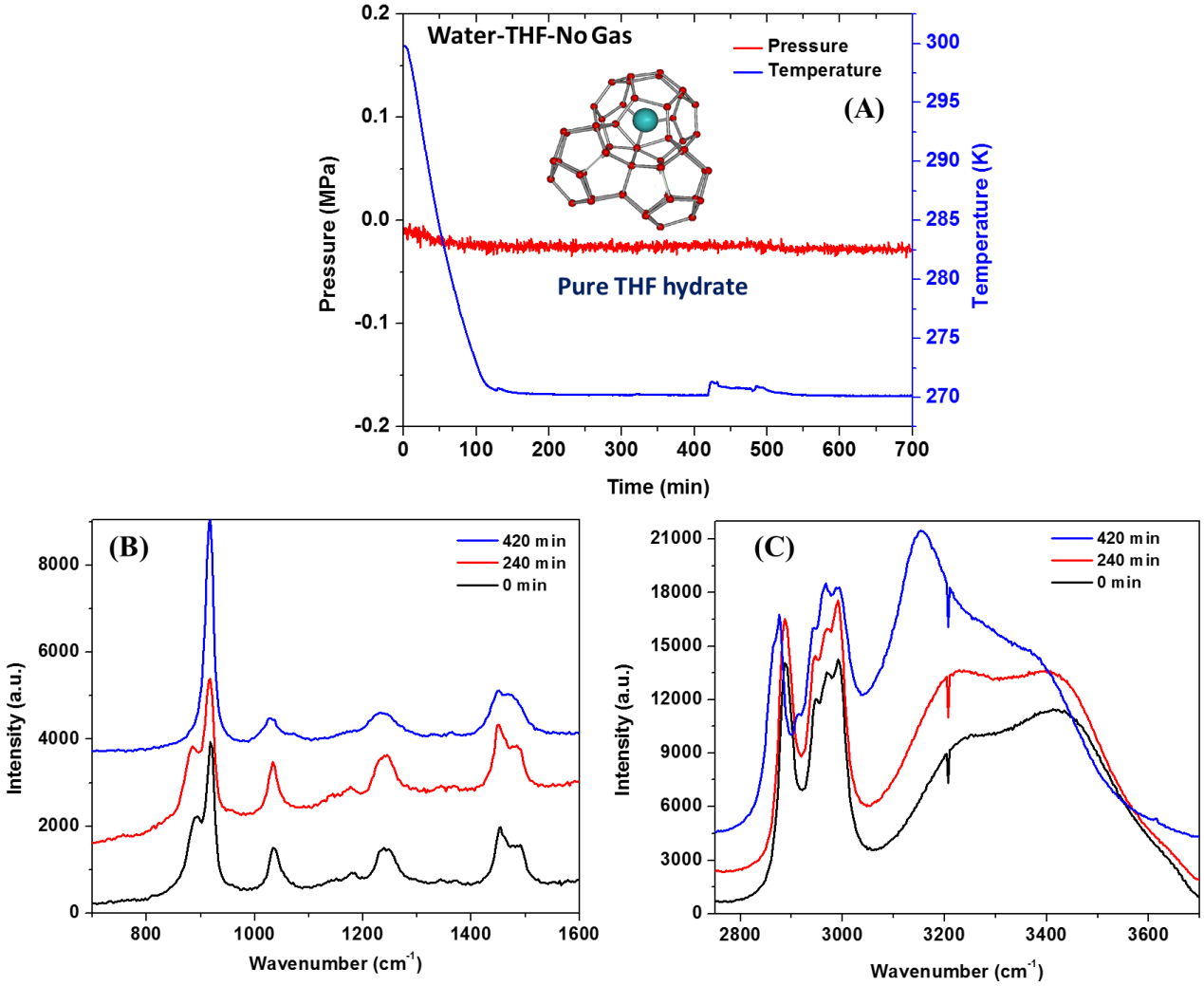

Figure S8. Pure THF hydrate formation for water+5.56 mol% THF system at atmospheric pressure and 270 K temperature in an unstirred reactor configuration. (A) Pressure and temperature profile during the THF hydrate formation (B) and (C) corresponding Raman spectra taken at different time interval during THF hydrate formation for C-C, C-O-C and C-H stretching region respectively. *(Note: Thermocouple was in gaseous phase in this experiment).* Related to the In-situ Raman investigations during Pure THF hydrate formation section (Figure 2 and 3 discussion) in results and discussion.

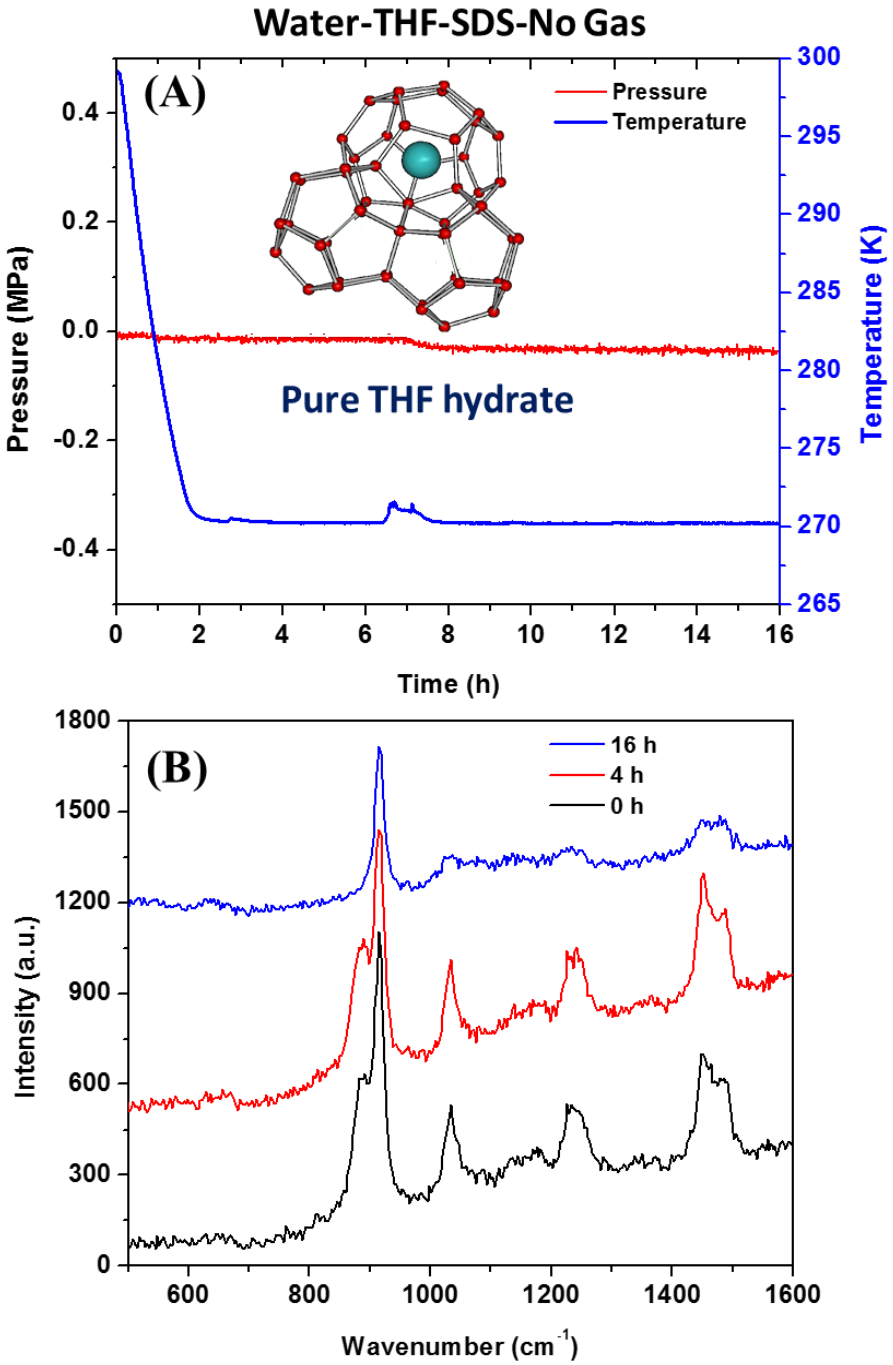

Figure S9. Pure THF hydrate formation for water+5.56 mol% THF+100 ppm SDS system at atmospheric pressure and ~270 K temperature in an unstirred reactor configuration. (a) Pressure and temperature profile during the THF hydrate formation (b) corresponding Raman spectra taken at different time interval during THF hydrate formation. *(Note: Thermocouple was in gaseous phase in this experiment)*. Related to the In-situ Raman

investigations during Pure THF hydrate formation section (Figure 2 and 3 discussion) in results and discussion.

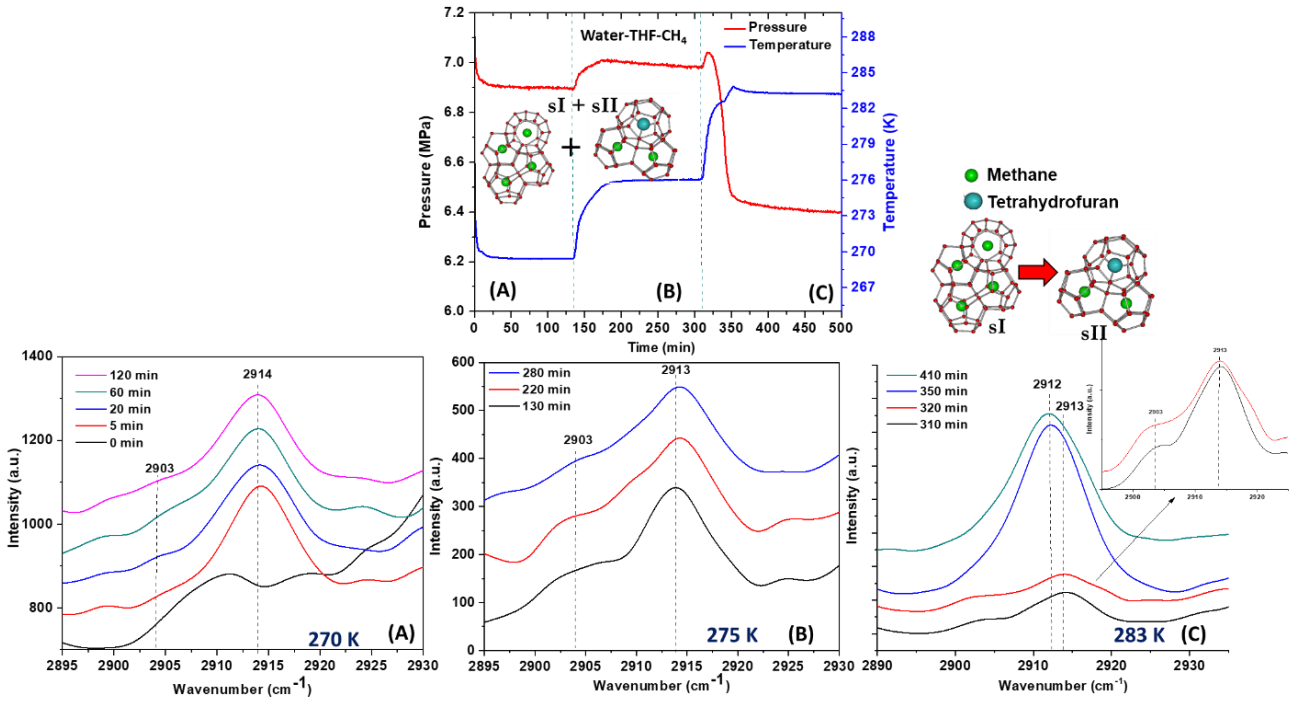

Figure S10. Pressure-Temperature profile of an experiment conducted in a UTR configuration using 5.56 mol% THF (no SDS). In which section (A) presents insertion of methane at 7.0 MPa and 270 K temperature into the previously formed pure THF hydrates and fig.S10A shows the corresponding Raman spectra for the occupancy of methane in small (2914 cm^{-1}) and large cages (2904 cm^{-1}). Section (B) and Fig. S10B show the rise in temperature to 275 K and the corresponding Raman spectra. Section (C) presents the melting of pure THF hydrates by rising the temperature up to 283 K and simultaneously formation of mixed THF-CH_4 hydrates (sII hydrates, shift in Raman peak from 2914 to 2912 cm^{-1}) (Rapid pressure drop and changes in the characteristic Raman peaks, see Figure S10C). *(Note: Thermocouple was in gaseous phase in this experiment).* Related to the In-situ Raman investigations during mixed CH_4-THF hydrate formation section (Figure 2 and 3 discussion) in results and discussion.

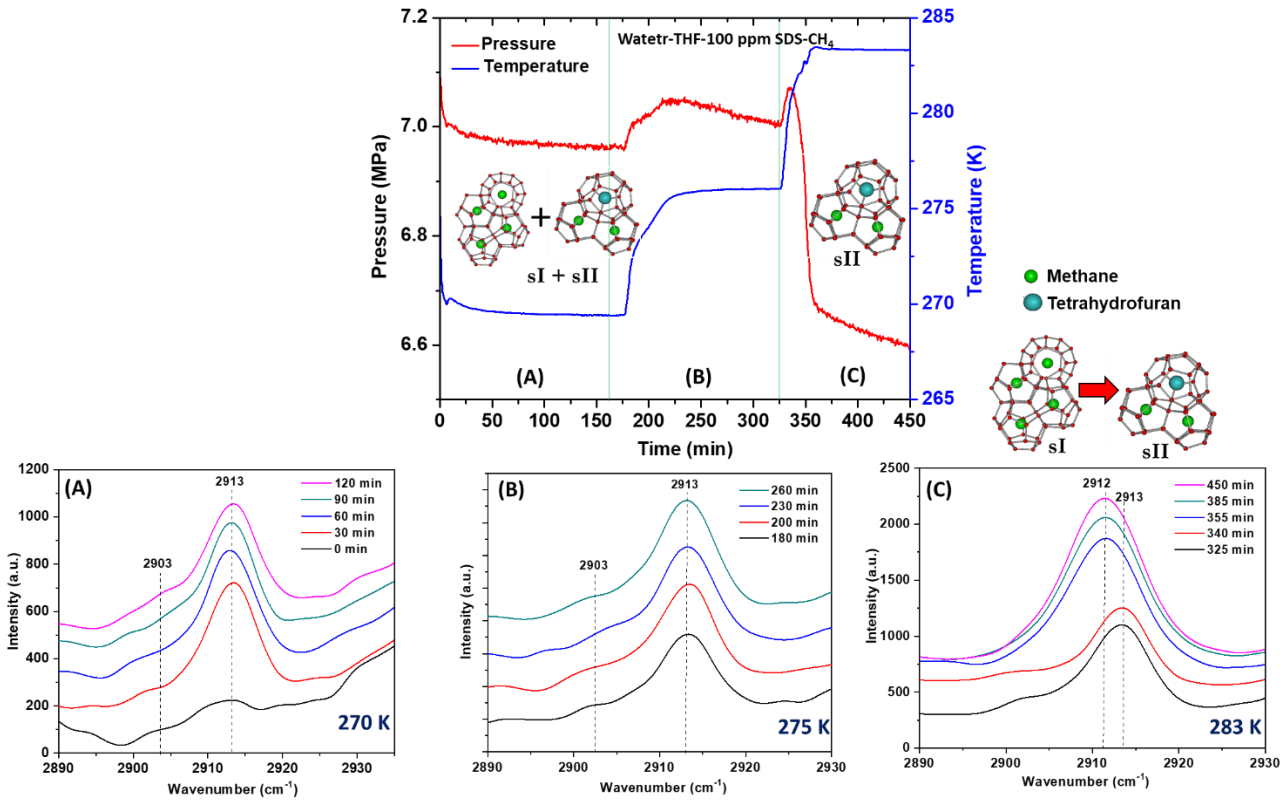

Figure S11. Pressure-Temperature profile of an experiment conducted in a UTR configuration using 5.56 mol% THF and 100 ppm SDS. In which section (A) presents insertion of methane at 7.0 MPa and 270 K temperature into the pure THF hydrates and fig.S11 A shows the corresponding Raman spectra for the occupancy of methane in small (2914 cm^{-1}) and large cages (2904 cm^{-1}). Section (B) and Fig. S11B show the rise in temperature to 275 K and the corresponding Raman spectra. Section (C) presents the melting of pure THF hydrates by rising the temperature up to 283 K and simultaneously formation of mixed THF-CH_4 hydrates (sII hydrates, shift in Raman peak from 2914 to 2912 cm^{-1}) (Rapid pressure drop and changes in the characteristic Raman peaks, see Figure S11C). *(Note: Thermocouple was in gaseous phase in this experiment).* Related to the In-situ Raman investigations during mixed CH_4-THF hydrate formation section (Figure 2 and 3 discussion) in results and discussion.

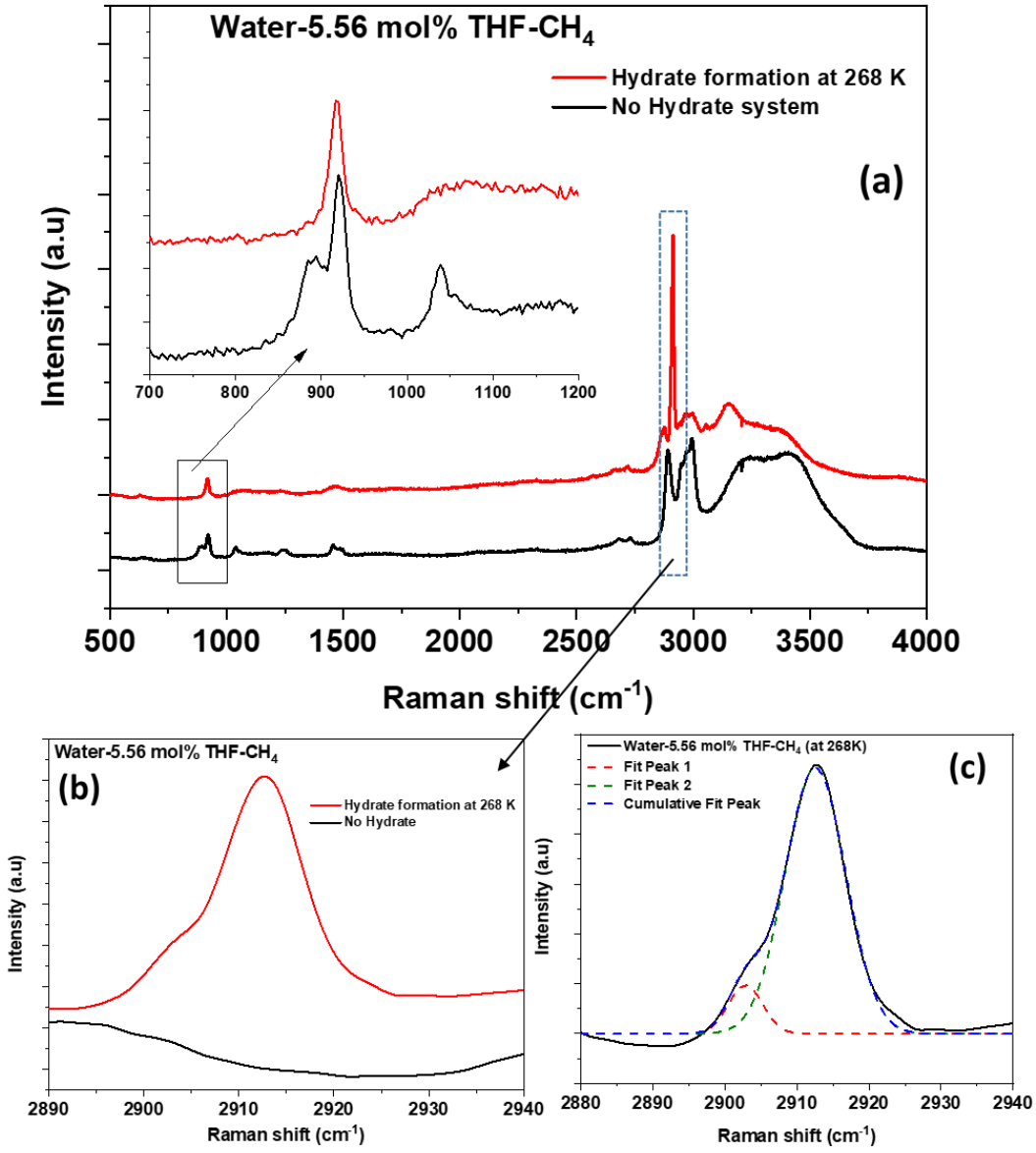

Figure S12. (a) Raman spectra (full spectral range) obtained for an experiment conducted in a UTR configuration (precooled at 268K) using 5.56 mol% THF at 7.2 MPa (b) Specific peaks for the occupancy of methane in small (2914 cm^{-1}) and large cages (2904 cm^{-1}). (c) Peak fitting to distinguish the small and large cage peaks. (Refer to procedure#2, experimental section). Related to Figure 8 discussion in results and discussion section.

SUPPLEMENTAL REFERENCES

Daraboina, N., Malmos, C., and von Solms, N. (2013). Investigation of Kinetic Hydrate Inhibition Using a High Pressure Micro Differential Scanning Calorimeter. Energy & Fuels *27*, 5779-5786.

Daraboina, N., Ripmeester, J., Walker, V.K., and Englezos, P. (2011). Natural Gas Hydrate Formation and Decomposition in the Presence of Kinetic Inhibitors. 1. High Pressure Calorimetry. Energy & Fuels *25*, 4392-4397.

Davies, S.R., Hester, K.C., Lachance, J.W., Koh, C.A., and Dendy Sloan, E. (2009). Studies of hydrate nucleation with high pressure differential scanning calorimetry. Chemical Engineering Science *64*, 370-375.

Hong, S.Y., Lim, J.I., Kim, J.H., and Lee, J.D. (2012). Kinetic Studies on Methane Hydrate Formation in the Presence of Kinetic Inhibitor via in Situ Raman Spectroscopy. Energy & Fuels *26*, 7045-7050.

Kumar, A., Daraboina, N., Kumar, R., and Linga, P. (2016). Experimental Investigation To Elucidate Why Tetrahydrofuran Rapidly Promotes Methane Hydrate Formation Kinetics: Applicable to Energy Storage. The Journal of Physical Chemistry C.

Kumar, A., Vedula, S.S., Kumar, R., and Linga, P. (2018). Hydrate phase equilibrium data of mixed methane-tetrahydrofuran hydrates in saline water. The Journal of Chemical Thermodynamics *117*, 2-8.

Kumar, A., Veluswamy, H.P., Kumar, R., and Linga, P. (2019a). Direct use of seawater for rapid methane storage via clathrate (sII) hydrates. Applied Energy *235*, 21-30.

Kumar, A., Veluswamy, H.P., Linga, P., and Kumar, R. (2019b). Molecular level investigations and stability analysis of mixed methane-tetrahydrofuran hydrates: Implications to energy storage. Fuel *236*, 1505-1511.

Le Parlouër, P., Dalmazzone, C., Herzhaft, B., Rousseau, L., and Mathonat, C. (2004). Characterisation of gas hydrates formation using a new high pressure Micro-DSC. Journal of Thermal Analysis and Calorimetry *78*, 165-172.

Lee, J.M., Cho, S.J., Lee, J.D., Linga, P., Kang, K.C., and Lee, J. (2015). Insights into the Kinetics of Methane Hydrate Formation in a Stirred Tank Reactor by In Situ Raman Spectroscopy. Energy Technology *3*, 925-934.

Seo, Y., Lee, J.-W., Kumar, R., Moudrakovski, I.L., Lee, H., and Ripmeester, J.A. (2009). Tuning the Composition of Guest Molecules in Clathrate Hydrates: NMR Identification and Its Significance to Gas Storage. Chemistry – An Asian Journal *4*, 1266-1274.

Veluswamy, H.P., Kumar, A., Premasinghe, K., and Linga, P. (2017). Effect of guest gas on the mixed tetrahydrofuran hydrate kinetics in a quiescent system. Applied Energy *207*, 573-583.